

Contents lists available at ScienceDirect

### Journal of Energy Chemistry

journal homepage: www.elsevier.com/locate/jechem



http://www.journals.elsevier.com/

# Catalytic activity of Cu/ZnO catalysts mediated by MgO promoter in hydrogenation of methyl acetate to ethanol

Fang Zhang a,b,c, Zhiyang Chen a,b,c, Xudong Fang a,b,c, Hongchao Liu a,b, Yong Liu a,b,\*, Wenliang Zhu a,b,\*

- a National Engineering Laboratory for Methanol to Olefins, Dalian Institute of Chemical Physics, Chinese Academy of Sciences, Dalian 116023, Liaoning, China
- b Dalian National Laboratory for Clean Energy, Dalian Institute of Chemical Physics, Chinese Academy of Sciences, Dalian 116023, Liaoning, China
- <sup>c</sup> University of Chinese Academy of Sciences, Beijing 100049, China

#### ARTICLE INFO

#### Article history: Received 22 January 2021 Revised 26 February 2021 Accepted 5 March 2021 Available online 26 March 2021

Keywords: Methyl acetate Hydrogenation Cu/ZnO catalyst MgO promoter Precursor effect Aurichalcite

#### ABSTRACT

Hydrogenation of methyl acetate is a key step in ethanol synthesis from dimethyl ether carbonylation and Cu-based catalysts are widely studied. We report here that the hydrogenation activity of Cu/ZnO catalysts can be enhanced by the addition of MgO promoter. The evolution of crystal phases during coprecipitation and the physicochemical properties of calcined and reduced catalysts by X-ray diffraction (XRD), thermogravimetric (TG)-mass spectrometry (MS), Brunauer-Emmett-Teller (BET), transmission electron microscopy (TEM), N<sub>2</sub>O titration, in situ CO-Fourier transform infrared spectroscopy (FTIR) and H<sub>2</sub>-temperature programmed reduction (H<sub>2</sub>-TPR) reveal that the promoter effect likely lies in the presence of Mg<sup>2+</sup>. A proper amount of Mg<sup>2+</sup> mediates the precipitation process of Cu and Zn, leading to preferable formation of aurichalcite  $(Cu_xZn_{1-x})_5(CO_3)_2(OH)_6$  crystal phase and a small amount of basic carbonates such as hydrozincite  $Zn_5(CO_3)_2(OH)_6$  and malachite  $Cu_2CO_3(OH)_2$ . The presence of aurichalcite strengthens the interaction between Cu and Zn species, and thus enhances the dispersity of Cu<sup>0</sup> species and helps generation of Cu<sup>+</sup> species on reduced catalysts. Furthermore, the performance of Cu/ZnO catalysts exhibits an optimal dependence on the Mg loading, i.e., 17.5%. However, too much Mg<sup>2+</sup> in the precipitation liquid prohibits formation of aurichalcite but enhances formation of basic nitrates, leading to a dramatically reduced hydrogenation activity. These findings may find applications for optimization of other Cu-based catalysts in a wider range of hydrogenation reactions.

© 2021 Science Press and Dalian Institute of Chemical Physics, Chinese Academy of Sciences. Published by ELSEVIER B.V. and Science Press. All rights reserved.

#### 1. Introduction

Ethanol is an important basic chemical, widely used for production of other chemicals such as acetyldehyde and ethylamine, and commodities such as painting and detergent. It is also a clean fuel additive for gasoline, which can significantly reduce the emission of hydrocarbons and  $NO_x$  [1]. Conventionally, ethanol is produced via fermentation and ethylene hydration [2]. With the increasing price for grains and decreasing oil reserves, it is desirable to develop alternative ethanol production technologies [3]. Although coal conversion to ethanol via syngas has been under investigation for decades, direct syngas conversion is still limited by its selectivity and the necessity of noble metal catalysts. In comparison, syngas via dimethyl ether (DME) carbonylation to ethanol is an attractive alternative due to its high efficiency and no requirement

E-mail addresses: yongl@dicp.ac.cn (Y. Liu), wlzhu@dicp.ac.cn (W. Zhu).

for noble metal catalysts although it involves multi-steps, i.e., syngas to DME, DME carbonylation to methyl acetate (MAc), followed by hydrogenation [4–7].

As one of the key steps in the above ethanol synthesis technology, hydrogenation of MAc determines the final product selectivity and has been extensively studied. Cu-based catalysts are the most efficient because they are selective towards C=O but exhibit almost no activity toward C=C [1,8–15]. Shen et al. [11] reported a MAc conversion of 96.2% and ethanol selectivity of 61.7% over Cu/SiO<sub>2</sub> catalysts at reaction conditions of 528 K, 1.0 MPa, and H<sub>2</sub>/MAc = 28. Ma et al. [12] studied Cu/ZnO/SBA-15 and the MAc conversion and ethanol selectivity of 96.1% and 94.9% were obtained, respectively at 493 K, 3.0 MPa, H<sub>2</sub>/MAc = 17.6 and liquid hourly space velocity (LHSV) = 1.8 h<sup>-1</sup>. Significant progress has been made in both industrial applications, and fundamental understanding of the active sites and the reaction mechanism. The mechanistic and kinetic study of MAc hydrogenation showed that the adsorbed MAc decomposed to methoxy and acetyl species first

<sup>\*</sup> Corresponding authors.

on the surface of Cu catalysts. The methoxy group was transformed to methanol under hydrogen while the hydrogenation of strongly adsorbed acetyl group to ethanol was considered to be the rate-determining step [11]. It was generally accepted that the synergetic effects of Cu<sup>0</sup> and Cu<sup>+</sup> and hence a proper ratio Cu<sup>+</sup>/Cu<sup>0</sup> were essential for a high activity. H<sub>2</sub> was activated over Cu<sup>0</sup> and MAc was transformed to methoxy and acetyl species over Cu<sup>+</sup> [16,17].

Wide studies demonstrated that the catalyst support and additives can have a significant effect on the structure and properties of Cu based catalysts, hence their activities [18–21]. For instance, the dispersity of Cu was reported to be improved by supporting Cu on MgO. MgO was also used as a promoter over Cu/SiO2 for MAc hydrogenation and Cu/ZnO for methanol and DME synthesis because it is similarly charged as Zn<sup>2+</sup> and its ion radius is smaller than Cu<sup>2+</sup> by only 2% [22]. For instance, Guo et al. [9] reported MgO promoted Cu/SiO<sub>2</sub> for MAc hydrogenation, which gave a conversion 80.3% and selectivity of ethanol 99% under reaction conditions of 613 K, 3.0 MPa,  $H_2/MAc = 10$ , LHSV = 2.0  $h^{-1}$  and the enhanced performance was attributed to fine copper dispersion, large amount of weakly basic sites and Cu<sup>+</sup> species. In addition, use of MgO as a support of Cu catalyst was also found to facilitate furfural conversion to furfuryl alcohol and its conversion and furfuryl alcohol selectivity reached as high as ~97% under conditions of H<sub>2</sub>/furfural (FAL) = 16, LHSV = 1.0  $h^{-1}$  [23]. Cui et al. [24] used Mg promoted CuAl catalyst with a layered double hydroxide (LDH) structure and achieved a high activity at a temperature as low as 438 K for hydrogenation of dimethyl oxalate to ethyl glycol as its yield reached 94.4%. The enhanced activity was attributed to the synergetic effects of the highly dispersed metallic Cu species and Lewis acid/base of the support, where H<sub>2</sub> was activated over the highly dispersed Cu<sup>0</sup> species and dissociation of C=O over MgO/ Al<sub>2</sub>O<sub>3</sub>. It is worthy to note that Cu<sup>+</sup> species were not detected over the reported Cu/MgO and CuMgAl catalysts.

We wonder if MgO could have a similar effect on Cu/ZnO catalysts in MAc hydrogenation, which has not been studied yet. Therefore, we prepared a series of MgO promoted Cu/ZnO by varying the loading of MgO. The systematic studies with X-ray diffraction (XRD), thermogravimetric (TG)-mass spectrometry (MS), N<sub>2</sub> adsorption, transmission electron microscopy (TEM), N<sub>2</sub>O titration, in situ CO-Fourier transform infrared spectroscopy (FTIR) and H<sub>2</sub>-temperature programmed reduction (H<sub>2</sub>-TPR) indicate that the presence of MgO mediates the precipitation forming preferably certain auricalchite precursor, which enhances metallic Cu dispersion and generation of Cu<sup>+</sup> species. Therefore, the hydrogenation of methyl acetate to ethanol is facilitated.

#### 2. Experimental

#### 2.1. Catalyst preparation

Cu/ZnO and Cu/ZnO/MgO were prepared by coprecipitation using metal nitrate and sodium carbonate as the precursors in a micro-impinging stream reactor, adapted from previous reports [25,26]. The molar ratio of Cu/Zn was 2/3. Briefly, a certain concentration of mixed metal nitrate solution including Cu, Zn, Mg and sodium carbonate solution were fed to the micro-impinging stream reactor through two constant-flux pumps at the same flow rate (100 mL/min) at 343 K and pH≈8.1. Subsequently, the suspension was quickly transferred into a water bath of 348 K under vigorous stirring. After the color of suspension had changed from blue to green, the aging was allowed for another 0.5 h, followed by filtering and washing with deionized water thoroughly until no Na<sup>+</sup> was detected. After being dried at 383 K for 12 h, the sample was calcined at 723 K for 4 h. The resulting catalysts were named

as  $Mg_xCuZn$  with x representing the molar loading of MgO while the un-promoted was denoted as CuZn.

#### 2.2. Catalyst characterization

The catalyst compositions were analyzed by X-ray fluorescence (XRF) (Philips Magix-601). Powder XRD was carried out over a PANalytical X'Pert PRO analytical diffractometer using Cu-K $_{\alpha}$  radiation ( $\lambda$  = 1.54 Å), operated at 40 kV and 40 mA. XRD patterns were recorded from  $2\theta$  = 10° to 80°. For characterization of reduced catalysts, in situ passivation in 1%  $O_2/N_2$  was carried out on the reduced catalyst. The crystal size was estimated using Scherrer equation.

The weight loss of the catalyst precursor was measured by thermogravimetric analysis (TGA, SDT Q600) and the effluents were monitored by an online MS. The signals were recorded while the temperature was raised from room temperature to 1067 K at a heating rate of 10 K/min in a flowing air stream.

 $N_2$  adsorption/desorption experiments were conducted at 77 K over a Micromeritics ASAP 2000 apparatus. The specific surface area was calculated from the isotherms by the Brunauer-Emmett-Teller (BET) method, and the pore size distribution was calculated by the Barrett-Joyner-Halenda (BJH) method from the desorption isotherms. Prior to measurements, the samples were subjected to evacuation at 623 K for 5 h.

TEM was carried out over a JEM-2100 system and FEI Titan Cubed Themis G3 300 (ETEM) electron microscope equipped with a field emission gun. The grounded sample was dispersed in ethanol under ultrasonic treatment and dipped onto the carbon-coated molybdenum grids.

The dispersity and the surface area of metallic Cu species were measured by  $N_2O$  titration over Micromeritics ASAP 2920 apparatus, by referring to a previously reported procedure [27]. Briefly, the catalyst was heated to 623 K at 10 K/min in 5%  $H_2$ /Ar, and then the temperature was decreased to 363 K in He. After being purged for 30 min by He, the catalyst was exposed to 10%  $N_2O$ /He (30 mL/min) for 0.5 h to ensure that the surface Cu atoms were completely oxidized to  $Cu_2O$ . Then He was introduced again to purge the system and the catalyst for 30 min. Following that, the catalyst was subjected to a second round reduction by increasing the temperature to 623 K at 10 K/min in 5%  $H_2$ /Ar. The integrated area of  $H_2$  consumption and its molar amount during the first round reduction were defined as  $A_1$  and X while those during the second round reduction as  $A_2$  and Y, respectively. Then the dispersity of metallic Cu species can be estimated according to the following equation:

$$D = \frac{2A_2}{A_1} \times 100\%.$$

The average diameter (d) of copper particles was calculated from  $A_1$  and  $A_2$  by assuming  $1.46 \times 10^{19}$  copper atoms per m<sup>2</sup> and a molar stoichiometry of N<sub>2</sub>O/Cu<sup>s</sup> = 0.5, where Cu<sup>s</sup> denotes the copper atoms on the surface [11,16,27]. The surface area of metallic Cu species  $(S_{\text{Cu}})$  can be estimated according to the following equation:

$$d = \frac{0.5A_1}{A_2} = \frac{1}{D},$$

$$\label{eq:cu} S_{\text{Cu}} = \frac{2 \textit{N}_{\text{A}} \times \textit{Y}}{\textit{X} \times 1.46 \times 10^{19} \times \textit{M}_{\text{Cu}} \times \textit{Wt}_{\text{Cu}} \%},$$

where  $M_{Cu}$ ,  $Wt_{Cu}$ % and  $N_A$  represent the molar mass of Cu, the mass percentage of Cu in the catalysts (determined by XRF) and the Avogadro constant, respectively [11,16,27].

*In situ* FTIR of CO adsorption was performed to identify surface Cu<sup>+</sup> species [16,27,28]. Prior to IR experiments, the sample was

reduced *in situ* for 1.5 h at 623 K under 20% H<sub>2</sub>/N<sub>2</sub> atmosphere, followed by cooling down to 363 K, and then N<sub>2</sub> purging for 1.5 h. Subsequently, 10% CO/N<sub>2</sub> was introduced to allow CO adsorption until the spectrum does not exhibit obvious change. Then the catalyst was purged by N<sub>2</sub> until no obvious change of the spectrum was observed.

 $H_2\text{-}TPR$  was carried out on the Micromeritics ASAP 2920 apparatus. Prior to the measurement, the catalysts were purged in He at room temperature for 0.5 h. Then they were heated in 10%  $H_2/Ar$  from room temperature up to 773 K at a heating rate of 10 K/min while the profiles were recorded.

#### 2.3. Catalytic reaction

MAc hydrogenation was carried out in a fixed-bed stainless steel tubular reactor with an inner diameter of 9 mm. 1.5 g catalyst (20–40 mesh) was loaded into the constant temperature section of a stainless steel reactor and reduced in situ under 20% H<sub>2</sub>/N<sub>2</sub> at 523 K, 0.1 MPa for 2 h. After the reduction was completed, the catalyst was cooled to the reaction temperature. Then the atmosphere of the reactor was displaced by hydrogen for three times. Following that, the reactor was pressurized with H<sub>2</sub> to 5.0 MPa, which was controlled by a back pressure regulator. MAc was injected through a high-pressure constant flow pump, and the pipeline was insulated to keep the temperature constant at 413 K to ensure vaporized MAc. The reaction was carried out at 473 K, 5.0 MPa, H<sub>2</sub>/ MAc = 5 and LHSV =  $1.0 h^{-1}$ . The effluents were analyzed by an online gas chromatograph (Agilent 7890A) equipped with a thermal conductivity detector, a flame ionization detector, TDX-01 and HP-PLOT/Q columns. The conversion of MAc ( $C_{MAc}$ ) and selectivity of product A (Sel<sub>A</sub>) were calculated using the following formula:

$$C_{\text{MAc}} = \frac{\text{Moles of feed MAc} - \text{Moles of MAc in the product}}{\text{Moles of feed MAc}} \times 100\%$$

$$Sel_{A} = \frac{\text{Moles of A formed}}{\text{Moles converted MAc}} \times 100\%$$

#### 3. Results and discussion

#### 3.1. Catalytic activity of MgO promoted Cu/ZnO in MAc hydrogenation

Fig. 1 shows that MAc conversion and ethanol selectivity increase stepwise with MgO loadings. An optimum activity was observed at MgO loading 17.5% (Mg<sub>17.5</sub>CuZn), i.e., conversion 89.8% and ethanol selectivity 86.7%. Then the activity drops abruptly at a MgO loading higher than 17.5%. For instance, it drops to 61.1% at a MgO loading 24.5% (Mg<sub>24.5</sub>CuZn) and 54.3% at 34.0% loading (Mg<sub>34.0</sub>CuZn). During MAc hydrogenation, ethanol may undergo transesterification with MAc leading to formation of ethyl acetate byproduct [3]. Fig. 1 displays that this byproduct is suppressed upon introduction of the MgO promoter and Mg<sub>17.5</sub>CuZn gives the lowest selectivity of ethyl acetate. The rest product selectivity is lower than 0.3%.

#### 3.2. Physicochemical properties of MgO promoted Cu/ZnO

It is well known that the physicochemical properties of Cu/ZnO catalyst can be significantly affected by many parameters during precipitation including the chemical composition, pH value, temperature and aging. Particularly, it was shown that the synthesis parameters during the very early stages of the precipitation could mediate the properties of the precursor and hence affect the catalytic activity of the final catalyst, so called "precursor effect" or

"chemical memory" [29-31]. We looked into the structural evolution using XRD upon the introduction of MgO promoter. Fig. 2 shows that the precipitates of CuZn, Mg<sub>5.8</sub>CuZn, Mg<sub>10.0</sub>CuZn and  $Mg_{17.5}CuZn$  contain aurichalcite  $(Cu_xZn_{1-x})_5(CO_3)_2(OH)_6$ , hydrozincite  $Zn_5(CO_3)_2(OH)_6$  and malachite  $Cu_2CO_3(OH)_2$  crystal phases. Formation of zincian malachite in the precipitates was widely considered to be most active for methanol synthesis and water-gasshift reaction [29]. Herman et al. [32] observed a single crystal phase of aurichalcite over the methanol synthesis catalysts with Cu/Zn molar ratio of 30/70. When the Cu/Zn molar ratio decreases below 30/70, a mixed phase of hydrozincite and aurichalcite was observed. Interestingly, over our MgxCuZn catalyst which has a molar ratio Cu/Zn = 2/3, the aurichalcite phase is dominant, accompanied by a small amount of malachite and hydrozincite in Fig. 2. In the aurichalcite phase, Zn prefers to locate in the tetrahedron center while Cu prefers to occupy the octahedron center. Thus, the close interaction of Cu and Zn species was proposed to be essential for a good dispersion of these species after calcination because the tetrahedron and octahedron alternate on the crystal fringe [100], as reported by Herman et al. [32]. With the increasing loading of MgO promoter, the diffraction peaks of malachite and hydrozincite weaken gradually and almost vanish over Mg<sub>17.5</sub>-CuZn. Further increasing MgO loading, the crystal phases of the precipitates change completely, i.e., no more basic carbonates and basic nitrates appearing. The above results show that the auricalcite crystal phase in the precipitates appear to be more active for MAc hydrogenation. Since the preparation procedure and the conditions have been the same except the loading of MgO, the significantly different crystal phases during precipitation can be attributed to the addition of different amount of MgO. The presence of too much Mg<sup>2+</sup> may hinder the inter-dispersion between Cu<sup>2+</sup> and Zn<sup>2+</sup>, and hence prohibits formation of aurichalcite phase during precipitation. Instead, it leads to formation of much less active basic nitrates

To further understand the effect of MgO promoter, we analyzed the catalysts with TG. The weight loss curves in Fig. 3 show that the more MgO the catalyst contains, the higher weight loss during TG. Their differential curves indicate that the catalysts containing less than 17.5% MgO only differ in the amount of weight loss, but the two main weight loss peaks are located in the same range of 500–650 K and 650–750 K. However, when MgO loading is higher than 24.5%, the weight loss occurs in the range of 475–550 K and 550–625 K over Mg<sub>24.5</sub>CuZn while 500–550 K and 650–725 K over

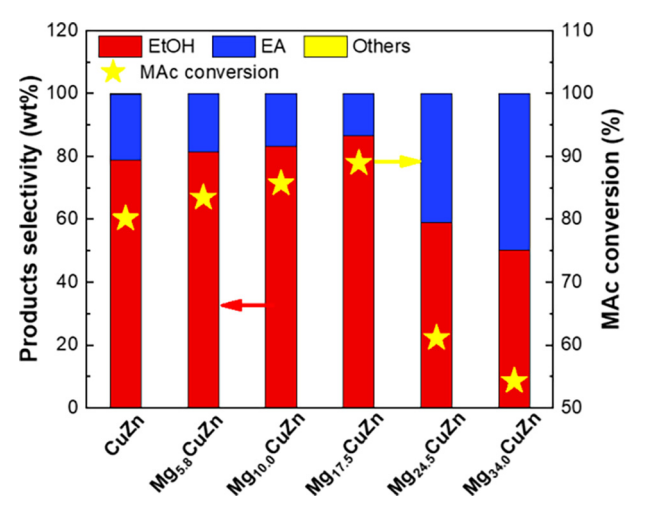


**Fig. 1.** Catalytic performance of Mg<sub>x</sub>CuZn catalyst in hydrogenation of MAc. Reaction conditions: catalysts loading = 1.5 g, T = 473 K, P = 5.0 MPa, H<sub>2</sub>/MAc = 5, LHSV = 1 h<sup>-1</sup>.

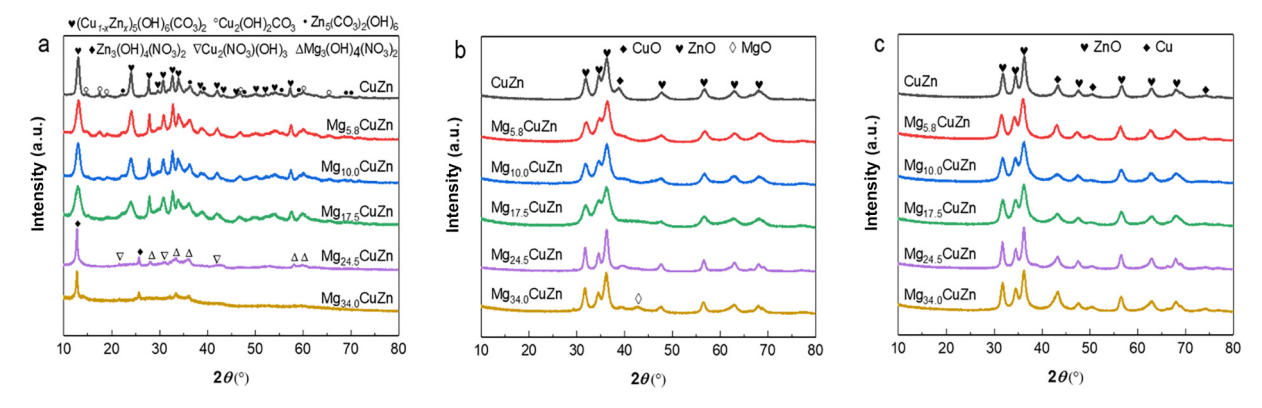


Fig. 2. XRD patterns of Mg<sub>x</sub>CuZn catalysts. (a) Precursors; (b) calcined catalysts; (c) reduced catalysts.

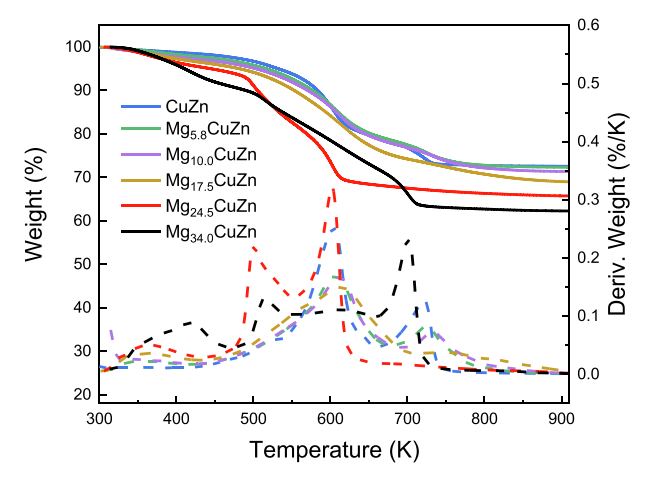


Fig. 3. Thermal gravity analysis of Mg<sub>x</sub>CuZn precursors.

Mg<sub>34.0</sub>CuZn, which could be attributed to the change of precursor composition and hence the crystal phases.

We employed an online mass spectrometer to monitor the effluents during TG analysis. As shown in Fig. 4, nitric oxide is

detected in the effluents during decomposition of the precursor of  $Mg_{24.5}CuZn$  and  $Mg_{34.0}CuZn$ . It agrees well with XRD, which detects the presence of basic nitrate crystals in the precipitates of those catalysts. For those containing less than 17.5% Mg, both  $CO_2$  and  $H_2O$  signals are detected in the same temperature range, which can be attributed to the decomposition products of basic carbonate. The above results confirm that the addition of MgO promoter mediates the coprecipitation process of Cu and Zn, and a proper amount of MgO promoter induces formation of aurichalcite crystal phase, accordingly enhancing the catalytic performance for MAc hydrogenation.

The XRD patterns of calcined catalysts in Fig. 2(b) show the diffraction of CuO, characterized at  $2\theta=38.7^\circ$ . This diffraction peak disappears over Mg<sub>17.5</sub>CuZn. However, it shows up again beyond 24.5% MgO. The characteristic ZnO diffraction peaks at 31.8°, 34.4° and 36.2° show a similar trend as that of CuO, weaken with the increasing MgO loading and intensify again beyond 24.5% MgO. The characteristic diffraction of MgO ( $2\theta=42.5^\circ$ ) starts to be discernible only above 34.0% MgO. Further analysis by Scherrer equation shows the addition of MgO reduces the crystal sizes of both CuO and ZnO (Table 1). Mg<sub>17.5</sub>CuZn exhibits the smallest crystal size for CuO and ZnO over the calcined catalyst and metallic Cu over the reduced one in comparison to the other MgO promoted

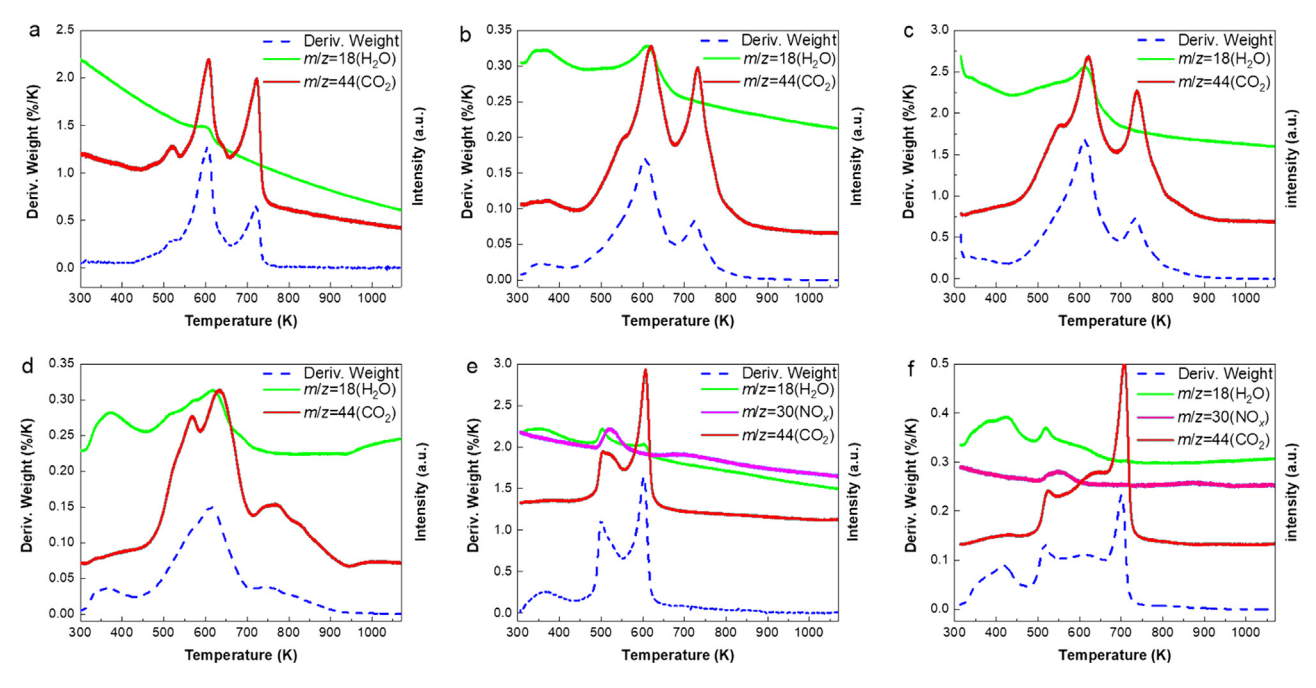


Fig. 4. Effluents monitored by an online mass spectrometer during TG analysis of  $Mg_xCuZn$  precursors. (a) CuZn; (b)  $Mg_{5.8}CuZn$ ; (c)  $Mg_{10.0}CuZn$ ; (d)  $Mg_{17.5}CuZn$ ; (e)  $Mg_{24.5}CuZn$ ; (f)  $Mg_{34.0}CuZn$ .

**Table 1**Composition and physicochemical properties of MgO promoted Cu/ZnO catalysts.

Catalyst	Content (mol%) <sup>a</sup>			$S_{\rm BET} ({\rm m}^2/{\rm g})$	D <sub>pore</sub> (nm)	V <sub>pore</sub> (cm <sup>3</sup> /g)	Cu dispersion <sup>b</sup> (%)	$S_{\text{Cu}}^{\text{b}} (\text{m}^2/\text{g})$	d <sup>b</sup> (nm)	D (nm) <sup>c</sup>		
	CuO	ZnO	MgO							CuO	Cu	ZnO
CuZn	40.8	59.2	_	49.5	20.6	0.26	10.9	36.8	9.2	8.1	7.4	12.1
Mg <sub>5.8</sub> CuZn	36.2	58.0	5.8	89.6	14.6	0.33	10.8	33.1	9.3	6.6	6.6	9.8
Mg <sub>10.0</sub> CuZn	36.9	53.1	10.0	108.4	12.4	0.34	17.1	35.0	5.8	5.8	5.4	10.2
Mg <sub>17.5</sub> CuZn	33.1	49.4	17.5	94.6	16.7	0.40	17.6	47.9	5.7	$ND^{d}$	5.2	9.6
Mg <sub>24.5</sub> CuZn	29.8	45.7	24.5	59.8	19.3	0.30	9.8	28.3	10.2	7.4	6.7	14.4
Mg <sub>34.0</sub> CuZn	25.7	40.3	34.0	64.3	18.4	0.30	11.1	29.5	9.0	10.9	6.0	12.5

- <sup>a</sup> Determined by XRF analysis.
- <sup>b</sup> Cu dispersion, surface area of metallic Cu<sup>0</sup> species (representated by  $S_{Cu}$ ) and the average diameter (d) of copper particles were determined by  $N_2O$  titration.
- <sup>c</sup> Crystal size (D) was estimated by Scherrer equation according to the XRD data.
- d Not detected

catalysts. These results unambiguously reveal the enhanced dispersion of Cu and ZnO species in the presence of a proper amount of MgO. Furthermore, the chemisorption of  $N_2O$  validates the highest dispersion and surface area of metallic Cu species over the reduced  $Mg_{17.5}CuZn$  among all the studied catalysts. These highly dispersed  $Cu^0$  species should play an important role in the reaction, which was reported in ester hydrogenation [16,17]. However, a simple linearly correlation between the MAc hydrogenation activity and the surface area of  $Cu^0$  species is not been observed as shown in Table 1 and Fig. 1. Interestingly, the BET surface areas of  $Mg_{10.0}CuZn$  and  $Mg_{17.5}CuZn$  are also the highest among the studied catalysts, in accordance with their Cu dispersion and their catalytic activity (Table 1).

## 3.3. Identification of surface Cu<sup>+</sup> species over MgO promoted Cu/ZnO catalysts

Further characterization with TEM shows that the lattice fringes corresponding to characteristic ZnO (101), (100) are frequently observed over CuZn,  $Mg_{17.5}CuZn$  and  $Mg_{34.0}CuZn$  (Fig. 5a–c). However, those of  $Cu^0$  species are not observed except  $Mg_{17.5}CuZn$ . Interestingly, we observe the lattice fringe of  $Cu_2O$  (110) (d=0.30 nm) over the reduced CuZn and  $Mg_{17.5}CuZn$  (Fig. 5a and d), indicating that CuO can be partially reduced to  $Cu_2O$  in 20%  $H_2/N_2$  at 523 K for 2 h. However, this is not observed over  $Mg_{34.0}CuZn$  after carefully examining the whole microscopic specimen (Fig. 5e).

To further confirm the presence of Cu<sup>+</sup> species over the reduced catalysts, we employed IR spectroscopy, which has been widely used to characterize the Cu species and their valence state [28,33,34]. Although the adsorption mode for CO on Cu<sup>+</sup> is still under debate, it is generally agreed that CO adsorption on Cu<sup>2+</sup> appears at a higher wave number than CO adsorption on Cu<sup>+</sup>, and further higher than CO on Cu<sup>0</sup> [28,35]. It is also agreed that CO adsorption on Cu<sup>2+</sup> and Cu<sup>0</sup> is reversible above 300 K, for example, CO-Cu<sup>0</sup> (CO adsorbed on Cu<sup>0</sup>) readily decomposes beyond the temperature range of 298-373 K and while CO-Cu<sup>+</sup> (CO adsorbed on Cu<sup>+</sup>) was rather stable and does not decompose even at 373 K [34]. Therefore, we used CO as a probe molecule for in situ FTIR to identify Cu<sup>+</sup> species on reduced catalysts. Prior to IR experiments. H<sub>2</sub>-TPR was carried out to identify the reduction temperature to ensure complete reduction of Cu species. The H<sub>2</sub>-TPR profiles in Fig. 6 show that the reduction temperature in general increases stepwise with the increasing loading of MgO, except Mg<sub>10.0</sub>CuZn and Mg<sub>17.5</sub>CuZn, which do not exhibit much change. This reveals more difficult to be reduced with the increasing loading of MgO. This implies that the presence of MgO likely has strengthened the interaction of Cu with ZnO/MgO, which hinders the reduction of Cu species. Nevertheless, reduction is completed at 623 K even over the Mg<sub>34.0</sub>CuZn catalyst. Thus all catalysts were reduced at 623 K prior to IR study.

CO adsorption was allowed for 30 min at 363 K. The spectra were only recorded after the *in situ* reactor had been swept by

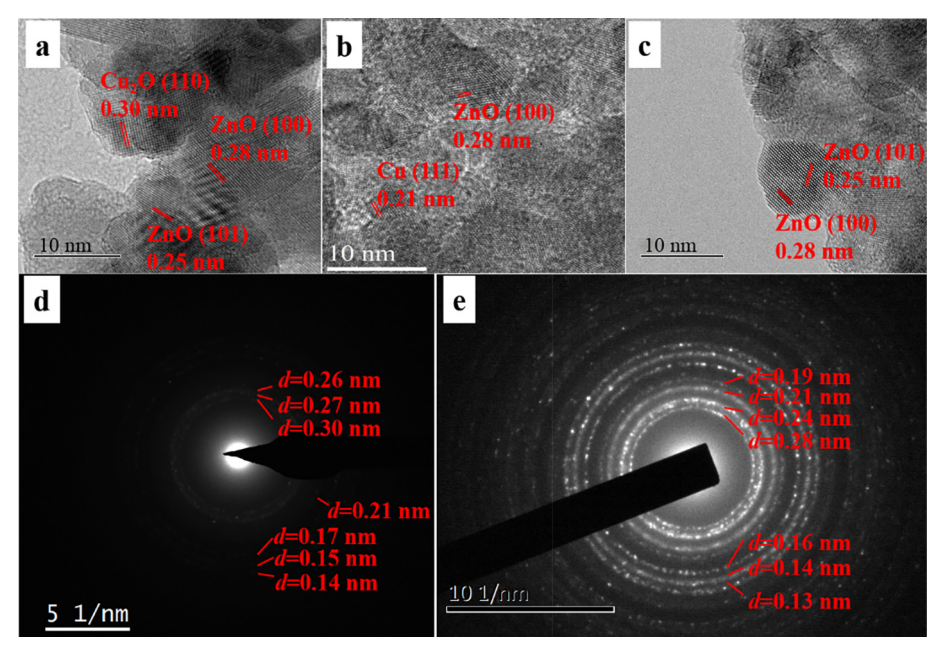


Fig. 5. TEM images of the reduced catalysts: (a) CuZn, (b) Mg<sub>17.5</sub>CuZn, (c) Mg<sub>34.0</sub>CuZn; electron diffraction images of the reduced catalysts: (d) Mg<sub>17.5</sub>CuZn, (e) Mg<sub>34.0</sub>CuZn.

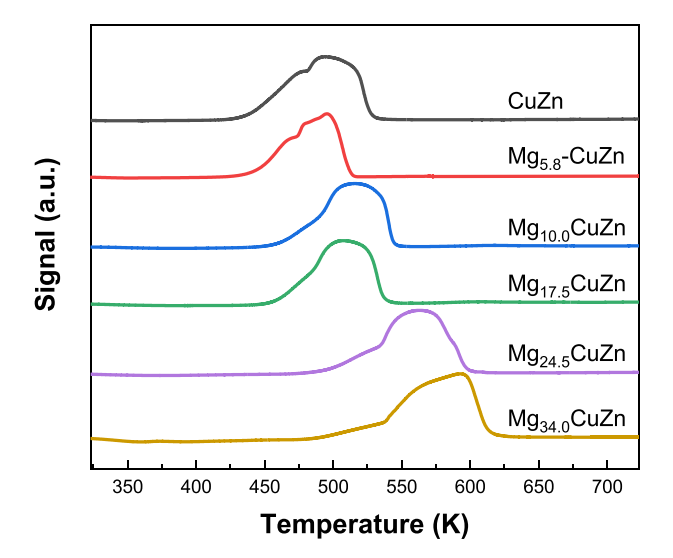


Fig. 6. H<sub>2</sub>-TPR profiles of MgO promoted Cu/ZnO catalysts.

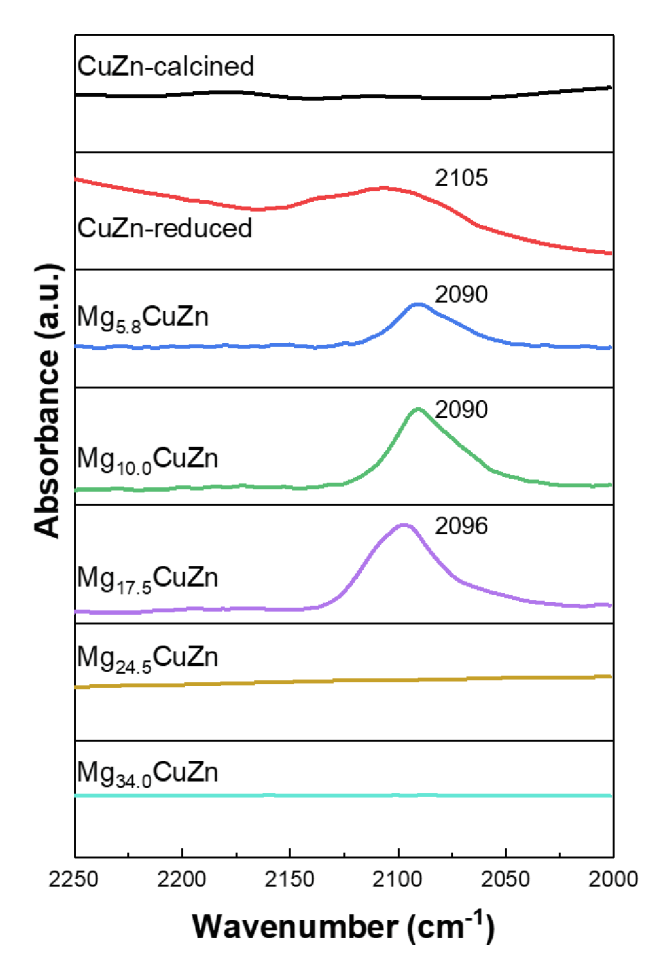


Fig. 7. In situ FTIR spectra of CO adsorption on MgO promoted Cu/ZnO catalysts at 363 K.

N<sub>2</sub> for 20 min. Fig. 7 displays no absorption band over the calcined CuZn catalyst, validating the reversible CO adsorption on Cu<sup>2+</sup>. In comparison, a broad band around 2105 cm<sup>-1</sup> shows up over the reduced CuZn catalyst upon exposure to CO. Since CO adsorption on Cu<sup>0</sup> is reversible, it is reasonable to attribute the 2105 cm<sup>-1</sup> band to CO adsorption on Cu<sup>+</sup>, which is consistent with the observation reported by Dandekar et al. [28]. Fig. 7 further shows that

this band is intensified and slightly shifted toward to a lower wave number over the MgO promoted catalysts. The intensities of Mg<sub>10.0</sub>CuZn and Mg<sub>17.5</sub>CuZn are obviously higher than that over Mg<sub>5.8</sub>CuZn, which indicates a much higher concentration of Cu<sup>+</sup> than that over CuZn and Mg<sub>5.8</sub>CuZn catalysts. By contrast, the catalysts containing more than 24.5% MgO do not exhibit CO adsorption peak, implying that Cu species most likely exist as Cu<sup>0</sup> over  $Mg_{24.5}CuZn$  and  $Mg_{34.0}CuZn$ . The essential role of coexisting of Cu<sup>0</sup> and Cu<sup>+</sup> has been reported by Ma and co-workers [27], where Cu<sup>+</sup> sites were observed to be important for adsorption of methoxy and acyl species and Cu<sup>0</sup> for dissociative activation of H<sub>2</sub>. Meanwhile, they also addressed that there existed a minimum metallic Cu surface area [16]. Below that value, the catalytic activity of hydrogenation was linearly correlated with Cu<sup>0</sup> surface area; beyond that value, the activity was strongly affected by the available Cu<sup>+</sup> species. Fridman et al. [34] reported that Cu<sup>+</sup> species tended to form solid solution with ZnO due to the same electrons of Cu<sup>+</sup> and Zn<sup>2+</sup> and thus suppressed the reduction of Cu<sup>+</sup> species in H<sub>2</sub>. Therefore, the highest activity of Mg<sub>17.5</sub>CuZn among the studied catalyst can be attributed to the highest dispersity of Cu<sup>0</sup> and the coexisting Cu<sup>+</sup> species. This may be traced back to the presence of MgO during precipitation, which strengthens the interaction of Cu with ZnO/MgO (Fig. 6) and help generation of Cu<sup>+</sup> species and at the same time facilitates dispersion of Cu<sup>0</sup>. Herman et al. [32,36] demonstrated that aurichalcite precursor was beneficial for dispersion of CuO and ZnO during calcination and thus the higher dispersity of Cu<sup>0</sup> was obtained, which enhanced interaction between Cu and Zn species and generation of Cu<sup>+</sup> species. However, too much Mg<sup>2+</sup> may hinder the inter-dispersion of Cu<sup>2+</sup> with Zn<sup>2+</sup>, forming much less active basic nitrates during precipitation.

#### 4. Conclusions

This study demonstrates that MgO promotion is an effective strategy to enhance the catalytic activity of Cu/ZnO in hydrogenation of methyl acetate. The results show that there exists an optimal MgO loading of 17.5%, which yielded a single pass conversion 89.8% and ethanol selectivity 86.7% at conditions of 473 K, 5.0 MPa,  $H_2/MAc = 5$  and LHSV = 1.0  $h^{-1}$ . However, a loading higher than 17.5% leads to abruptly dropping activity. The presence of Mg<sup>2+</sup> can modulate the coprecipitation process of copper and zinc, leading to preferable formation of aurichalcite crystal phase accompanied by formation of a small amounts of basic carbonates such as hydrozincite  $Zn_5(CO_3)_2(OH)_6$  and malachite  $Cu_2CO_3(OH)_2$ . As a result, MgO helps generation of Cu<sup>+</sup> species and enhances the dispersion of metallic Cu species on reduced catalysts. The optimal performance of Mg<sub>17.5</sub>CuZn catalyst derived from aurichalcite precursor was ascribed to the highest dispersion of metallic copper and the coexisting Cu<sup>+</sup> species. These finding could guide further development of highly efficient Cu-based catalysts for hydrogenation of other esters.

#### **Declaration of Competing Interest**

The authors declare that they have no known competing financial interests or personal relationships that could have appeared to influence the work reported in this paper.

#### Acknowledgments

This work was supported from the National Natural Science Foundation of China (Grant Nos. 21972141, 21991094, 21991090), and the "Transformational Technologies for Clean Energy and Demonstration", Strategic Priority Research Program of the Chinese Academy of Sciences (Grant No. XDA21030100).

#### References

- [1] C. Gan, Y. Wang, C. Ye, C. Guo, Aust. J. Chem. 72 (2019) 417-424.
- [2] M. Balat, H. Balat, Appl. Energy 86 (2009) 2273–2282.
- [3] J. Goldemberg, Science 315 (2007) 808–810.
- [4] P. Cheung, A. Bhan, G.J. Sunley, E. Iglesia, Angew. Chem. Int. Ed. Engl. 45 (2006)
- [5] X. San, Y. Zhang, W. Shen, N. Tsubaki, Energy Fuels 23 (2009) 2843-2844.
- [6] A. Bagno, J. Bukala, G.A. Olah, J. Org. Chem. 55 (1990) 4284-4289.
- [7] J. Liu, H. Xue, X. Huang, Y. Li, W. Shen, Catal. Lett. 139 (2010) 33–37.
- [8] X. Li, X. San, Y. Zhang, T. Ichii, M. Meng, Y. Tan, N. Tsubaki, ChemSusChem 3 (2010) 1192–1199.
- [9] H. Qin, C. Guo, C. Sun, J. Zhang, J. Mol. Catal. A-Chem. 409 (2015) 79–84.
   [10] C. Ye, C. Guo, C. Sun, Y. Zhang, RSC Adv. 6 (2016) 113796–113802.
- [11] X. Huang, M. Ma, S. Miao, Y. Zheng, M. Chen, W. Shen, Appl. Catal. A-Gen. 531 (2017) 79-88.
- [12] Y. Wang, J. Liao, J. Zhang, S. Wang, Y. Zhao, X. Ma, AICHE J. 63 (2017) 2839–2849.
- [13] Y. Zhao, B. Shan, Y. Wang, J. Zhou, S. Wang, X. Ma, Ind. Eng. Chem. Res. 57 (2018) 4526-4534
- [14] Y. Zhang, C. Ye, C. Guo, C. Gan, X. Tong, Chin. J. Catal. 39 (2018) 99-108.
- [15] Y. Xi, Y. Wang, D. Yao, A. Li, J. Zhang, Y. Zhao, J. Lv, X. Ma, ChemCatChem 11 (2019) 2607-2614
- [16] J. Gong, H. Yue, Y. Zhao, S. Zhao, L. Zhao, J. Lv, S. Wang, X. Ma, J. Am. Chem. Soc. 134 (2012) 13922–13925.
- [17] X. Ma, Z. Yang, X. Liu, X. Tan, Q. Ge, RSC Adv. 5 (2015) 37581–37584.
  [18] I. Kasatkin, P. Kurr, B. Kniep, A. Trunschke, R. Schlögl, Angew. Chem. Int. Ed. Engl. 46 (2007) 7324–7327.
- [19] Z. Lu, H. Yin, A. Wang, J. Hu, W. Xue, H. Yin, S. Liu, J. Ind. Eng. Chem. 37 (2016) 208-215

- [20] J. Schumann, T. Lunkenbein, A. Tarasov, N. Thomas, R. Schlögl, M. Behrens, ChemCatChem 6 (2014) 2889–2897.
- [21] R.P. Ye, L. Lin, Q. Li, T. Wang, C.K. Russell, Z. Zhou, H. Adidharma, Z. Xu, Y.-G. Yao, M. Fan, Catal. Sci. Technol. 8 (2018) 3428-3449.
- [22] S. Asthana, C. Samanta, A. Bhaumik, B. Banerjee, R.K. Voolapalli, B. Saha, J. Catal. 334 (2016) 89-101.
- [23] H. Liu, Q. Hu, G. Fan, L. Yang, F. Li, Catal. Sci. Technol. 5 (2015) 3960-3969.
- [24] G. Cui, X. Meng, X. Zhang, W. Wang, S. Xu, Y. Ye, K. Tang, W. Wang, J. Zhu, M. Wei, D.G. Evans, X. Duan, Appl. Catal. B-Environ. 248 (2019) 394-404.
- [25] S. Kaluza, M. Muhler, Catal. Lett. 129 (2008) 287-292.
- [26] Q. Zhang, Z. Liu, X. Zhu, L. Wen, Q. Zhu, K. Guo, J. Chen, Ind. Eng. Chem. Res. 54 (2015) 8874-8882.
- Y. Wang, Y. Shen, Y. Zhao, J. Lv, S. Wang, X. Ma, ACS Catal. 5 (2015) 6200-6208.
- [28] A. Dandekar, M.A. Vannice, J. Catal. 178 (1998) 621-639.
- [29] M. Behrens, R. Schlögl, Z. Anorg, Allg. Chem. 639 (2013) 2683–2695.
- [30] I. Kim, G. Lee, H. Jeong, J.H. Park, J.C. Jung, J. Energy Chem. 26 (2017) 373–379.
- [31] T. Lunkenbein, F. Girgsdies, T. Kandemir, N. Thomas, M. Behrens, R. Schlögl, E. Frei, Angew. Chem. Int. Ed. Engl. 55 (2016) 12708-12712.
- [32] P.B. Himelfarb, G.W. Simmons, K. Klier, R.G. Herman, J. Catal. 93 (1985) 442-450.
- [33] M. Turco, G. Bagnasco, U. Costantino, F. Marmottini, T. Montanari, G. Ramis, G. Busca, J. Catal. 228 (2004) 43-55.
- [34] V.Z. Fridman, A.A. Davydov, J. Catal. 195 (2000) 20-30.
- [35] B.H. Sakakini, J. Tabatabaei, M.J. Watson, K.C. Waugh, J. Mol. Catal. A-Chem. 162 (2000) 297-306.
- [36] R.G. Herman, K. Klier, G.W. Simmons, B.P. Finn, J.B. Bulko, T.P. Kobylinski, J. Catal. 56 (1979) 407-429.